Identification of MCM4 and PRKDC as new regulators of osteosarcoma cell dormancy based on 3D cell cultures

Camille Jubelin, Javier Muñoz-Garcia, Emilie Ollivier, Denis Cochonneau, François Vallette, Marie-Françoise Heymann, Lisa Oliver, Dominique Heymann

BBA - Molecular Cell Research 1871 (2024) 119660

Contents lists available at ScienceDirect

BBA - Molecular Cell Research

journal homepage: www.elsevier.com/locate/bbamcr

Research Paper

Identification of *MCM4* and *PRKDC* as new regulators of osteosarcoma cell dormancy based on 3D cell cultures

Camille Jubelin [a,b,c], Javier Muñoz-Garcia [a,b], Emilie Ollivier [b], Denis Cochonneau [b], François Vallette [b,d], Marie-Françoise Heymann [a,b], Lisa Oliver [d,e], Dominique Heymann [a,b,f,*]

[a] Nantes Université, CNRS, US2B, UMR 6286, 44000 Nantes, France
[b] Institut de Cancérologie de l'Ouest, Tumor Heterogeneity and Precision Medicine Lab., 44805 Saint-Herblain, France
[c] Atlantic Bone Screen, 44800 Saint-Herblain, France
[d] Nantes Université, INSERM, CRCI²NA, UMR1307, 44000 Nantes, France
[e] CHU de Nantes, Nantes, France
[f] Department of Oncology and Metabolism, Medical School, University of Sheffield, Sheffield, UK

ARTICLE INFO

Keywords:
Osteosarcoma
Cell dormancy
Quiescency
Transcriptomic profile
3D spheroids

ABSTRACT

Dormancy is a potential way for tumors to develop drug resistance and escape treatment. However, the mechanisms involved in cancer dormancy remain poorly understood. This is mainly because there is no *in vitro* culture model making it possible to spontaneously induce dormancy. In this context, the present work proposes the use of three-dimensional (3D) spheroids developed from osteosarcoma cell lines as a relevant model for studying cancer dormancy. MNNG-HOS, SaOS-2, 143B, MG-63, U2OS and SJSA-1 cell lines were cultured in 3D using the Liquid Overlay Technique (LOT). Dormancy was studied by staining cancer cells with a lipophilic dye (DiD), and long-term DiD^+ cells were considered as dormant cancer cells. The role of the extracellular matrix in inducing dormancy was investigated by embedding cells into methylcellulose or Geltrex™. Gene expression of DiD^+ cells was assessed with a Nanostring™ approach and the role of the genes detected in dormancy was validated by a transient down-expression model using siRNA treatment. Proliferation was measured using fluorescence microscopy and the xCELLigence technology. We observed that MNNG-HOS, 143B and MG-G3 cell lines had a reduced proliferation rate in 3D compared to 2D. U2OS cells had an increased proliferation rate when they were cultured in Geltrex™ compared to other 3D culture methods. Using 3D cultures, a transcriptomic signature of dormancy was obtained and showed a decreased expression of 18 genes including *ETV4*, *HELLS*, *ITGA6*, *MCM4*, *PRKDC*, *RAD21* and *UBE2T*. The treatment with siRNA targeting these genes showed that cancer cell proliferation was reduced when the expression of *ETV4* and *MCM4* were decreased, whereas proliferation was increased when the expression of *RAD21* was decreased. 3D culture facilitates the maintenance of dormant cancer cells characterized by a reduced proliferation and less differential gene expression as compared to proliferative cells. Further studies of the genes involved has enabled us to envisage their role in regulating cell proliferation.

1. Introduction

Cancers are characterized by high inter- and intratumor heterogeneity. The dynamic and progressive aspect of this tumor heterogeneity, which is amplified under selection pressure (*i.e.* chemotherapy, immune system, hypoxia, *etc.*) allows cancer cells to adapt to their environment and is a major cause of therapeutic failure. Of the mechanisms used by cancer cells to survive, cancer dormancy may contribute to disease recurrence and the development of mechanisms of resistance to treatment. Cancer dormancy is a phenomenon during which the tumor stops its growth, sometimes for long periods, either because an equilibrium between proliferation and cell death is established (tumor mass dormancy), or because cancer cells stop or greatly slow their proliferation rate (cancer cell dormancy). During this dormancy period, the tumor mass is undetectable using conventional imaging approaches and dormant cells can progressively escape chemo- and/or radiotherapies that preferentially target highly proliferative cells.

Osteosarcoma is the most common primary bone cancer, with an incidence of 3–4.5 cases per million population per year. Half of osteosarcomas occurs in children and adolescents [1]. While localized forms

* Corresponding author at: Institut de Cancérologie de l'Ouest, Blvd Jacques Monod, 44805 Saint-Herblain, France.
E-mail address: dominique.heymann@univ-nantes.fr (D. Heymann).

https://doi.org/10.1016/j.bbamcr.2024.119660
Received 7 September 2023; Received in revised form 15 December 2023; Accepted 3 January 2024
Available online 10 January 2024

of osteosarcoma present a 5-year survival rate of over 70 %, this value drops to 30 % for patients with metastases [2,3]. Cases of cancer dormancy in the context of osteosarcoma have been described, and their frequency is probably associated with osteosarcoma recurrence rates (30 % for localized cancers, 90 % for disseminated cancers) [4]. Unfortunately, studying dormancy poses a major challenge, as clinically, it is only exposed when the disease recurs. Furthermore, *in vitro* models for pre-clinical research generally use cell lines selected for their ability to proliferate indefinitely in adherent monolayers, the opposite of a cancer dormancy phenotype. To investigate the factors responsible for cancer dormancy, it is therefore essential to use culture models that enable its spontaneous induction.

In this study, we highlighted the relevance of 3D cultures, and particularly spheroids, for studying cancer dormancy mechanisms in the context of osteosarcoma. The level of proliferation of several osteosarcoma lines was compared according to the culture method employed (2D or 3D), or the matrix used for spheroid generation and growth (matrix-free, methylcellulose or Geltrex™). Thanks to the use of 3D culture, a transcriptomic signature of dormancy was obtained. Further study of the genes involved has enabled us to envisage their role in regulating cell proliferation.

2. Materials & methods

2.1. Cancer cell lines and culture media

MNNG-HOS (CRL-1547, ATCC), 143B (91112502, ECACC), and MG-63 (CRL-1427, ATCC) osteosarcoma cell lines were cultured in DMEM 4.5 g/L D-glucose and 0.11 g/L sodium pyruvate (L0106-500, Dutscher, Bernolsheim, France) supplemented with 5 % fetal bovine serum (FBS) (CVFSVF00-01, Eurobio Scientific, Les Ulis, France) and 2 mM L-glutamine (25030-024, Gibco, Paris, France). The SaOS-2 (89050205, ECACC) and U2OS (HTB-96, ATCC) osteosarcoma cell lines were cultured in McCoy's 5A (P04-05500, PAN biotech, Aidenbach, Germany) supplemented with 10 % FBS and 2 mM L-glutamine. The SJSA-1 osteosarcoma cell line (Prof. S. Mittnacht) was cultured in RPMI (L0501-500, Dutscher, Bernolsheim, France) supplemented with 10 % FBS and 2 mM L-glutamine. All cell lines were regularly tested for the absence of mycoplasma.

2.2. 2D culture

Cell lines were maintained as adherent monolayers in T25 or T75 flasks. At 90 % confluency, cells were passaged, cells were passed following conventional cell maintenance protocols based on trypsin-EDTA detachment. To study cell proliferation and before siRNA transfection, cells were grown in flat-bottom 96-well adherent plates (3599, Corning Costar, Boulogne-Billancourt, France).

2.3. 3D culture

Spheroids were generated in low-adherence round-bottom 96-multiwell plates (174926, Thermo Scientific, Saint-Herblain, France) using the Liquid Overlay Technique (LOT) [5]. Cells were seeded at a concentration of 20,000 cells per 100 µL per well of 96-multiwells plates. After 24 h, 50 µL of complete culture medium was added to each well. The generation of spheroids was performed by using two steps. Firstly, detached cells initially cultured in 2D were resuspended at a concentration of 1×10^6 cells/mL. A solution of methylcellulose (HSC001, R&D System, Abington, UK) or Geltrex™ LDEV-Free Reduced Growth Factor (A14132-02, Gibco, Paris, France) was added to the cell suspension at a final concentration of 0.1× and 0.02× respectively. 25 µL droplets were then put on the inside of a Petri dish cover and incubated in the inverted position for 24 h at 37 °C. PBS was added to the Petri dish to avoid dehydration. Secondly, droplets with preformed spheroids were transferred to low adherence 96-multiwells plates, with one droplet-containing spheroid per well. Culture medium was added to reach a final volume of 150 µL, similar to LOT. Culture media were changed every 2–3 days by replacing 2/3 of the initial volume.

2.4. DiD labelling

On day 0, cell lines were labeled with the lipophilic dye Vybrant™ DiD Cell-labeling Solution (V22887, Invitrogen, Paris, France) according to the manufacturer's recommendations. After cell counting and resuspension at a density of 1×10^6 cells/mL in serum-free culture medium, the cells were incubated with 5 µL of DiD (dilution: 1/200) for 10 min at 37 °C, before undergoing three successive washes with serum-free medium. As the DiD dye is used as a proliferation marker, the labeled cells were manipulated in the absence of direct light to preserve maximum fluorescence. Under these conditions, fluorescence intensities can remain stable in non-dividing cell populations considered to be "dormant" cells, whereas they halved with each mitosis in dividing cell populations [6].

2.5. Cell viability assay

The viability of cells cultured in 3D was analyzed by two approaches: i) a global approach at the spheroid level by measuring the LDH release in cell cultures at various time points, ii) at the cellular level by flow cytometry by analyzing the 7-AAD staining in DiD^+ and DiD^- cell populations. Briefly, after 3D cell culture, 5 µL of the supernatant was taken from each well. This supernatant was diluted 1/20 in PBS, and 10 µL of this solution was added to 15 µL of LDH Storage buffer and 25 µL Enzyme Mix from the LDH-Glo™ Cytotoxicity Assay kit (J2380, Promega, Charbonnières-les-Bains, France). Each sample was put in the well of an opaque white 96-well plate. The plate was left at room temperature for 1 h in the dark. Afterward, luminescence rates were assessed using the VICTOR Nivo (Perkin Elmer, Villebon sur Yevette, France) plate reader. After enzymatic dissociation, DiD^+ and DiD^- cells were incubated with 5 µL of 7-AAD (00-6993-50, Invitrogen®, Paris, France) per 1×10^6 cells for 5 min, protected from light before being analyzed by flow cytometry.

2.6. Nucleus labelling of living cells

To count the number of total cells and/or DiD^+ cells with microscopy, cells were labeled with the fluorescent dye Hoechst 33342 (H3570, Invitrogen) that binds to DNA (excitation: 350 nm; emission: 461 nm). A stock solution of 0.01 µg/mL (1:5000) in PBS was prepared extemporaneously. 50 µL of this stock solution was added to the 100 µL of medium in the wells. Cells were incubated with the dye for 30 min to 1 h at 37 °C, protected from light. Before imaging, the cells were washed then covered with fresh culture medium.

2.7. Hematoxylin and eosin staining

The spheroids were embedded in Cryomatrix™ (6769006, Epredia, Runcorn, UK) for microscopic observation of the inner parts of the 3D-cultured cells. The assembly was snap-frozen in liquid nitrogen-cooled isopentane, and the frozen cytoblock was stored at −80 °C. Microtome sections of the cytoblocks were made in a cryostat with the chamber at −20 °C. The 3- to 6-µm-thick sections were placed on microscope slides before being stained and mounted. Sections were stained with hematoxylin and eosin (3801656/3801656CN, Leica, Nanterre, France), which stains the nucleus and matrix respectively. The sections were exposed for 1.5 min to hematoxylin, before being rinsed thoroughly with tap water. The sections were then immersed in eosin for one minute. Excess dye was rinsed off with tap water. Slides were then passed through 100 % alcohol twice, then dipped in a xylene bath 3 times before mounting.

2.8. Microscopy

Live cells were imaged using Perkin Elmer's Operetta CLS High-Content Analysis System microscope. Images were then analyzed using Harmony software. Slides of spheroid sections were imaged with a Nikon Eclipse Ni-U5 microscope.

2.9. siRNA transfection

MISSION® esiRNA was used for the transient sub-expression of human genes. siRNAs targeting the following genes of interest were used: si*ETV4* (EHU069441, Merck, Lyon Paris), si*HELLS* (EHU075091, Merck, Lyon, Paris), si*ITGA6* (EHU088861, Merck, Lyon, Paris), si*MCM4* (EHU081181, Merck, Lyon, Paris), si*PRKDC* (EHU123791, Merck, Lyon Paris), si*RAD21* (EHU108911, Merck, Lyon, Paris) and si*UBE2T* (EHU013731, Merck, Lyon, Paris). The siRNAs si*KIFF11* (EHU019931, Merck, Lyon, Paris) and si*EGFP* (EHUEGFP, Merck, Lyon, Paris) were used as positive and negative controls respectively. Cells were transfected with Lipofectamine™ RNAiMAX transfection agent (13778075, Thermo Scientific, Saint-Herblain, France) and OptiMEM® I medium (31985062, Thermo Scientific, Saint-Herblain, France). Transfection was performed by reverse transfection according to the supplier's recommendations, either with 10 nM siRNA for the individual treatment conditions, or with a 2 nM siRNA mixture for the pool condition (si*HELLS* + si*MCM4* + si*PRKDC* + si*RAD21* + si*UBE2T*). The down-expression of genes treated with the different siRNAs was validated by RTqPCR.

2.10. RNA extraction and RTqPCR

Total RNA from 2D-cultured MNNG-HOS cells was extracted with the NucleoSpin RNA Plus kit (700984, Macherey-Nagel, Hoerdt, Allemagne) by column purification according to the manufacturer's recommendations. RNA concentration was measured using a NanoDrop One. Reverse transcription of RNA into cDNA was performed using the OneScript RT Mix with g/DNAOut kit (OZYA012-100, Ozyme, Saint-Cyr-l'école, France) according to the manufacturer's recommendations. 100 ng of RNA was reverse transcribed per sample.

Expression of the *ETV4*, *HELLS*, *ITGA6*, *MCM4*, *PRKDC*, *RAD21* and *UB2ET* genes was assessed with qPCR. The sequences of the primers designed are described in Table 1. qPCR reactions were carried out using the PowerUp™ SYBR™ Green Master Mix (A25741, Applied Biosystem, California, US). Heating cycle conditions included 40 cycles divided into a denaturation step at 95 °C for 1 s and a hybridization step at 60 °C for 30 s. The extinction coefficient ε was calculated according to the formula:

$$\varepsilon = 100^{*}(2\hat{}(-\Delta\Delta Ct)\ CTRL - 2\hat{}(-\Delta\Delta Ct)\ EXP)$$

The change in gene expression was obtained by normalization with the *RPLPO* (QT00075012, QIAGEN, Manchester, UK) and *GAPDH* (QT00079247, QIAGEN) housekeeping genes.

Table 1
Primer sequences.

Gene	Primers
ETV4	Forward: 5′ CACCTTCAGCAGCAAATCGC 3′ Reverse: 5′ GATCTTCAGAGTCGAGGGGC 3′
HELLS	Forward: 5′ CATGCACAGCTTCAACACGG 3′ Reverse: 5′ ATCCGACTGGGGGTTCCAAT 3′
ITGA6	Forward: 5′ TGCCAGCAAGGTGTAGCAG 3′ Reverse: 5′ CTCTACACGAACAATCCCTTTCCA 3′
MCM4	Forward: 5′ CAACGGCATCTGCTGTATCG 3′ Reverse: 5′ CTGACAGATGATCCCAGCCTTT 3′
PRKDC	Forward: 5′ TGCCCCTCATCAGTGGTTTC 3′ Reverse: 5′ ACTCTTTGGACTAACTCCCTCG 3′
RAD21	Forward: 5′ ACTACTTTGGATCTGGCACCG 3′ Reverse: 5′ GACAGCGTGTAAAGAGCTTCAG 3′
UBE2T	Forward: 5′ ATTGCCACCAAAAGGTGCTTG 3′ Reverse: 5′ CAGGGTTGGGTTCTGACATGA 3′

2.11. Nanostring™ analysis

RNA from MNNG-HOS DiD^{-} and DiD^{+} cells was extracted using Macherey-Nagel's NucleoSpin RNA Plus XS kit (740990, Macherey-Nagel, Hoerdt, Allemagne) immediately after cell sorting by flow cytometry. RNA concentration was quantified on a NanoDrop. For Nanostring™ analysis, 50 ng of RNA in a maximum volume of 5 µL was required per sample. To analyze gene expression differences between DiD^{-} and DiD^{+} tumor cells, the NanoString PanCancer Human IO 360™ panel was selected. Hybridization of capture and reporter probes with target RNAs was performed according to the manufacturer's recommendations. The solution containing the RNA samples and probes was placed in a thermocycler at 65 °C for at least 16 h. Following hybridization, the samples were put in an automated nCounter Prep Station to remove excess probes and mRNA. The purified samples were then loaded on to a cartridge, where they could bind *via* the biotin of the capture probe. The fixed samples were then loaded into a second automated system, the nCounter Digital Analyze, a multi-channel epifluorescence scanner. The scanner took as many images as the number of reporter probes detected. These images were then converted into digital values for analysis. The data obtained were analyzed using Nanostring nSolver Analysis Software, and statistical tests were performed.

2.12. Cell proliferation

Cell proliferation was measured using the xCELLigence approach and compared with several control conditions: (i) untreated, (ii) treated only with transfection reagent (TR), (iii) treated with *eGFP* siRNA (siEGFP, transcript is not expressed by cells), and (iv) treated with *KIFF11* siRNA (siKIFF11) known to arrest proliferation and result in cell death over the long term. The results obtained are given as Cell Index (CI) normalized against time. The higher the CI, the more cells covered the well surface. The CI curve comprised several stages: i) an initial adhesion phase, followed by a period of exponential growth resulting in a linear positive slope; ii) a peak in CI corresponding to a slowdown and then a halt in proliferation, when the cells completely cover the well and have no more space to multiply and iii) a decreasing phase corresponding to cell death.

2.13. Statistical analysis

All experiments were carried out three times, in triplicate and data represent three independent biological replicates. Statistical analyses were performed using GraphPad Prism 7.0 software (GraphPad Software, La Jolla, CA, USA) and the statistical tests used are indicated in each figure legend. A p-value ≤ 0.05 was considered statistically significant.

3. Results

3.1. 3D culture diminished cell proliferation of osteosarcoma cell lines

After labeling with the lipophilic membrane dye DiD, 143B, MG-63 and MNNG-HOS cells were seeded in 2D or 3D in flat-bottom and round-bottom 96-well plates respectively. The proliferation rate was assessed using fluorescence microscopy after analysis of the cell viability (Fig. 1A-C and Supplementary Fig. 1). The analyses of the LDH release and 7-AAD staining demonstrated a very limited loss of viability in 3D cell cultures with >95 % of viable DiD^{+} ^{and} DiD^{-} cells at any time point of the cell culture (data not shown). Day 1 after seeding, most cells in each cell line was DiD^{+}, whether grown in 2D or 3D culture. Only MG-63 cells cultured in 2D showed a lower fraction of positive cells, at around 60 % (Fig. 1D). Over time, the level of DiD fluorescence and the number of DiD^{+} cells remained stable in the cell lines cultured in 3D. Conversely,

a drastic decrease in the number of DiD$^+$ cells was observed for all cell lines cultured in 2D as early as 5 days after seeding. At day 15, only a low number of MG-63 cells were still DiD$^+$ in 2D (Fig. 1B), and none for 143B and MNNG-HOS cells (Fig. 1A and C). 3D culture of osteosarcoma cell lines was therefore associated with slowed cell proliferation compared with 2D culture. This observation shows that 3D culture is an interesting model for studying the mechanism of tumor dormancy.

3.2. Osteosarcoma cell lines cultured in 3D display heterogeneous morphological profiles

Six osteosarcoma cell lines (143B, MG-63, MNNG-HOS, SaOS-2, SJSA-1 and U2OS) were grown in 3D for 15 days. Morphological parameters of the spheroids generated were compared: number of spheroids produced per well, cross-sectional area, minimum diameter, and roundness. Depending on the lineage, different morphological profiles were observed. Spheroids from 143B, MNNG-HOS and SJSA-1 were large, with a minimum diameter of over 500 µm throughout the entire culture period. In addition, these spheroids increased in size over time, approaching 750 µm in diameter by day 15. MG-63 spheroids were intermediate in size, maintaining a diameter of around 500 µm throughout the 15-day culture period (Fig. 2B and C). Finally, these four lines generated a single spheroid per well, with a high degree of roundness (Fig. 2A and D). Conversely, the SaOS-2 and U2OS lines failed to generate a single spheroid per well (Fig. 2A) and formed smaller spheroids than the other four cell lines (Fig. 2B and C). In particular, the cross-sectional area and minimum diameter of SaOS-2 spheroids fluctuated over time. Moreover, SaOS-2 and U2OS spheroids had much lower roundness values (Fig. 2D). Finally, the SaOS-2 and U2OS cell lines produced very dense spheroids, while the 143B, MG-63, MNNG-HOS and SJSA-1 cell lines formed spheroids of intermediate density with a dark core and lighter border (Fig. 2F and Supplementary Fig. 2). These results reveal that several osteosarcoma cell lines can form spheroids under the culture conditions used, but exhibit various morphological patterns. The 3D behavior of these lines could thus reflect their specific characteristics.

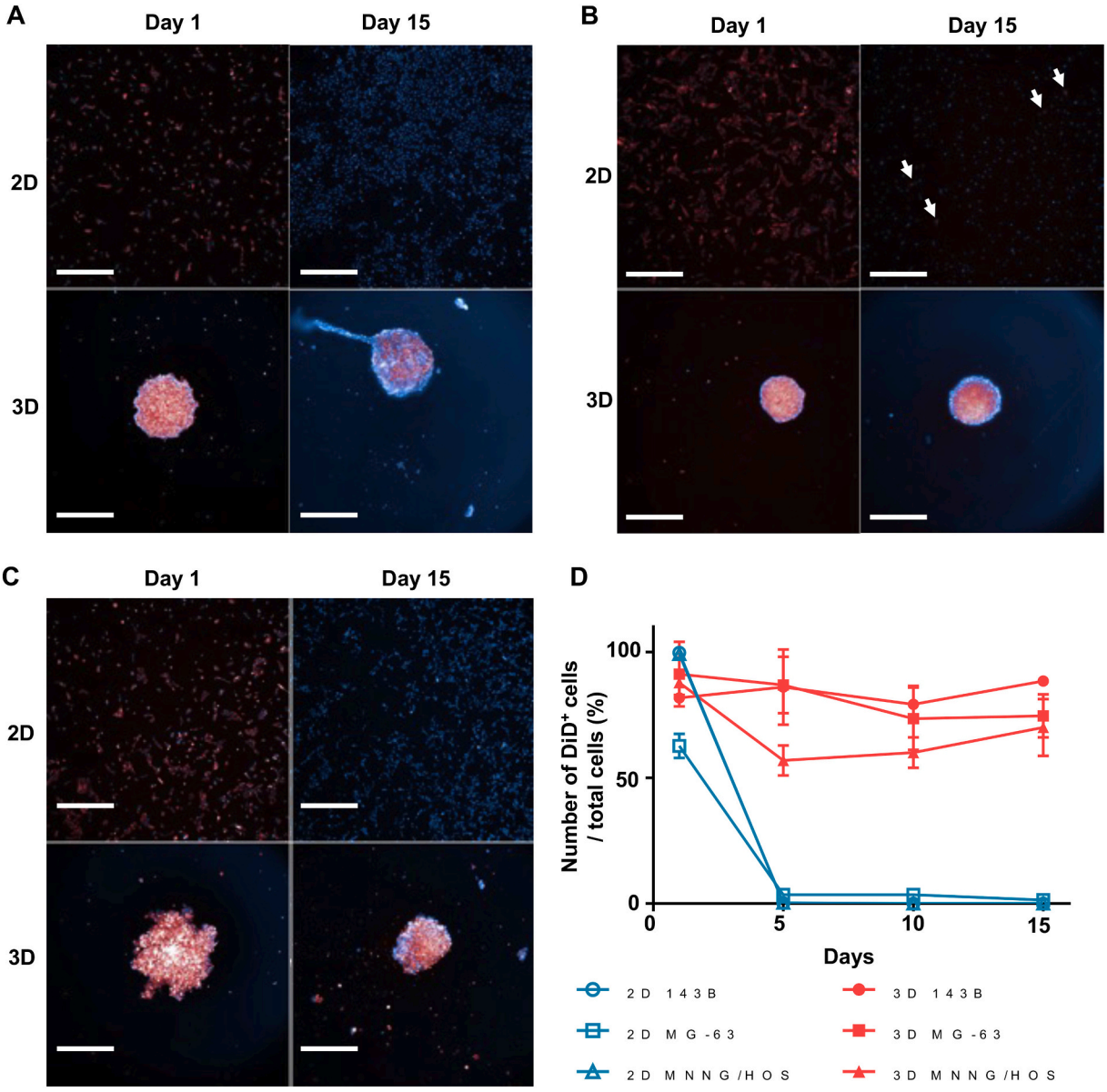

Fig. 1. Comparing DiD dilution between 2D and 3D cultures. 143B (**A**), MG-63 (**B**) and MNNG-HOS (**C**) cells were labeled with the lipophilic membrane dye DiD before being seeded in 2D or 3D in 96-well plates. DiD intensity (**A-C**) and the number of DiD$^+$ cells (**D**) over time were assessed with microscopy.

3.3. The tumor microenvironment plays a role in the cancer dormancy of osteosarcoma cells cultured in 3D

Of the cell lines studied previously, two osteosarcoma lines were selected to further investigate the role played by the extracellular matrix on cell proliferation: a large spheroid-forming cell line (MNNG-HOS) and a small spheroid-forming cell line (U2OS). Cells were labeled with DiD and cultured for 15 days either using LOT or HD embedded in 0.1 % methylcellulose or 0.02 % Geltrex™.

When the minimum diameter of MNNG-HOS spheroids was compared, no difference was observed between the three 3D culture methods (Fig. 3A). Conversely, an increase in minimum diameter was detectable from day 7 of culture for U2OS spheroids cultured in Geltrex™ compared with those grown using LOT or in methylcellulose (Fig. 3B). Interestingly, the average fluorescence of DiD expressed by U2OS spheroids after Day15 cultured in Geltrex™ showed a significant decrease in intensity compared to those grown using LOT (Fig. 3C and D). Thus, Geltrex™ produced larger U2OS spheroids suggesting more proliferating cells.

Microscopic observation of spheroids grown in Geltrex™ at Day15 showed that MNNG-HOS spheroids exhibited higher DiD fluorescence in the center of the sphere. Moreover, cytological analysis of the spheroids after HE stains revealed that cells were more numerous at the spheroid periphery (purple nucleus), while the core was richer in extracellular matrix (pale pink staining) (Fig. 3E). In the case of U2OS cells, the spheroids showed an alveolar organization, with spherical zones separated by fewer cell-dense grooves. The presence of large lacunae composed of extracellular matrix was also demonstrated (Fig. 3F). These results highlight the impact of the extracellular matrix on the spatial organization and cell proliferation of osteosarcoma cell lines.

3.4. Long-term culture of DiD$^+$ cells demonstrates differential transcriptomic profiles between positive and negative cells

After 35 days of culture, MNNG-HOS cells labeled with the lipophilic dye DiD were dissociated, and the cells sorted by flow cytometry based on the level of intensity of DiD fluorescence. Two cell populations were obtained: strongly positive DiD$^+$ cells representing around 15 % of the

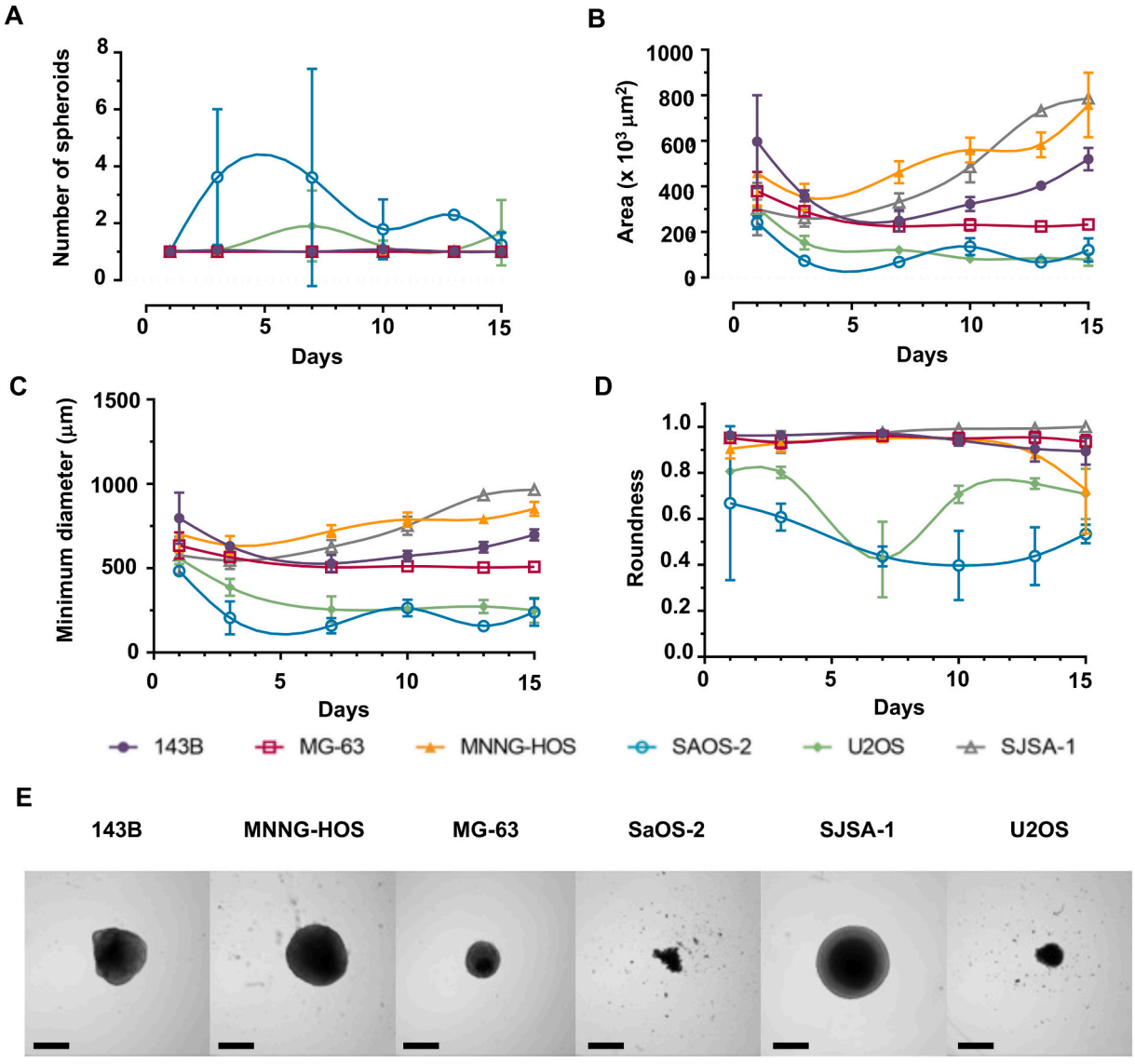

Fig. 2. Morphological characterization of osteosarcoma cell lines grown in 3D with LOT. Morphological parameters of the spheroids produced from 143B, MG-63, MNNG-HOS, SaOS-2, SJSA-1 and U2OS osteosarcoma cell lines. The number of spheroids per well (**A**), cross-sectional area (**B**), minimum diameter (**C**) and roundness (**D**) were measured with light microscopy coupled to image J software. The roundness was calculated by using the following formula: 4 x Area/(π x Major Axis^2). (**D**) Representative microscopy images of spheroids formed by the different lines 15 days after seeding. Scale bar = 500 µm.

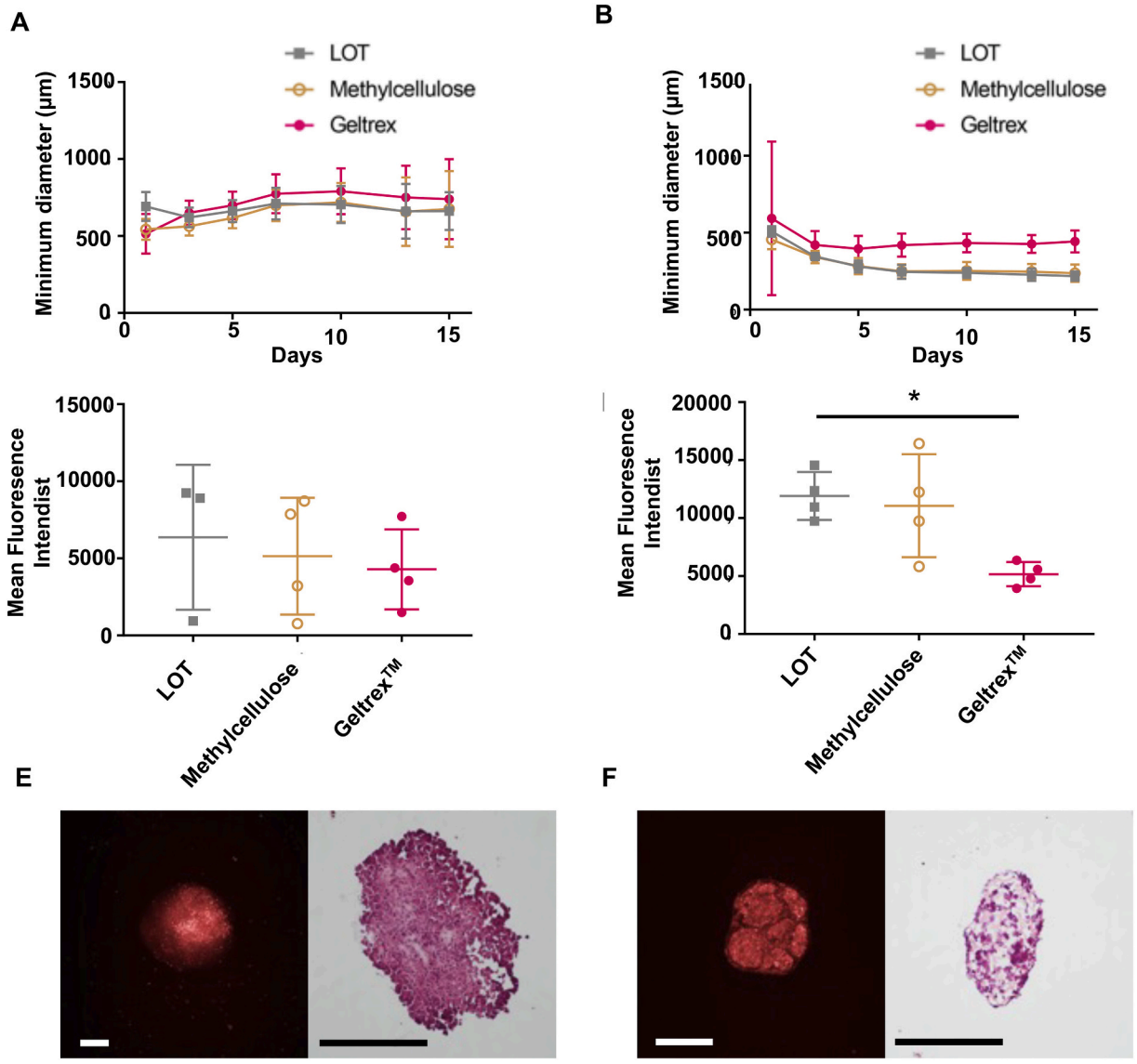

Fig. 3. Impact of the microenvironment on cancer cell dormancy. MNNG-HOS and U2OS cells were labeled with the lipophilic membrane dye DiD and cultured in 3D by LOT or embedded in extracellular matrices composed of methylcellulose or Geltrex™. (**A-B**) Measurement over time of the minimum diameter of MNNG-HOS and U2OS spheroids respectively. (**C—D**) Measurement of mean DiD fluorescence intensity 15 days after 3D seeding of MNNG-HOS and U2OS spheroids respectively. (**E-F**) Day 15 microscopy images of MNNG-HOS and U2OS spheroids respectively. Left: fluorescence microscopy image; DiD in red. Right: white light microscopy image; hematoxylin and eosin staining. Scale bar: 300 µm. Statistical test: Kruskal-Wallis; *p < 0.05.

total cells (Supplementary Fig. 3) and DiD^- cells that had no DiD staining. Transcriptomic analysis using the Nanostring™ approach compared the expression of over 700 genes involved in cancer between proliferating (DiD^-) and dormant (DiD^+) cells. Differential expression of 18 genes significantly under-expressed in DiD^+ cells was obtained (Fig. 4A). STRING analysis [7] of these 18 genes revealed that most of them interacted with each other at the protein level, either physically or functionally, with the exception of *NF2* and *ETV4* (Fig. 4B). Finally, the signaling pathways associated with the expression of these genes were evaluated (Fig. 4C). Half of the genes (*CCNA2*, *CCNB1*, *PTTG2*, *MCM4*, *PCNA*, *SKP2*, *PRKDC*, *SMC3*, *RAD21*) are involved in the cell cycle and apoptosis pathways. Other signaling pathways are also represented, such as the DNA damage and repair pathway (*UBE2T*, *PCNA*, *PRKDC*), chromatin modification (*HELLS*), cancer driver genes (*HIST1H3B*, *NF2*), the PI3K pathway (*SPP1*, *ITGA6*) and transcriptional deregulation mechanisms (*HIST1H3G*, *HIST1H3B*, *HIST1H3H*, *ETV4*). Taken together, these results suggest that the differentially expressed genes between DiD^+ cells and DiD^- cells fit a transcriptomic signature of dormancy.

3.5. Treatment of osteosarcoma cells with siRNA leads to altered cell proliferation

Among the list of genes identified in DiD^+ cancer cells, 7 of them (*ETV4*, *HELLS*, *ITGA6*, *MCM4*, *PRKDC*, *RAD21* and *UBE2T* genes) were selected based on a review of the literature. We then studied the contribution of each gene in the control of dormancy of osteosarcoma cell by using siRNA approach. In addition, due to their functional interaction (Supplementary Fig. 4), an equimolar mixture of 5 of these siRNAs (directed against the *HELLS, MCM4*, *PRKDC*, *RAD21* and *UBE2T* transcripts) named "Pool" was also assessed.

The functional efficacy of each siRNA was validated with RT-qPCR (Fig. 5A). We considered that an effective siRNA shed should be associated with a gene silencing coefficient of over 70 %. This extinction rate was reached 24 h after treatment for most siRNAs used at a concentration of 10 nM, with the exception of *PRKDC*. In the case of the latter, one of the experimental replicates did not appear to be correctly quenched by the siRNA, whereas extinction was over 80 % for the other two

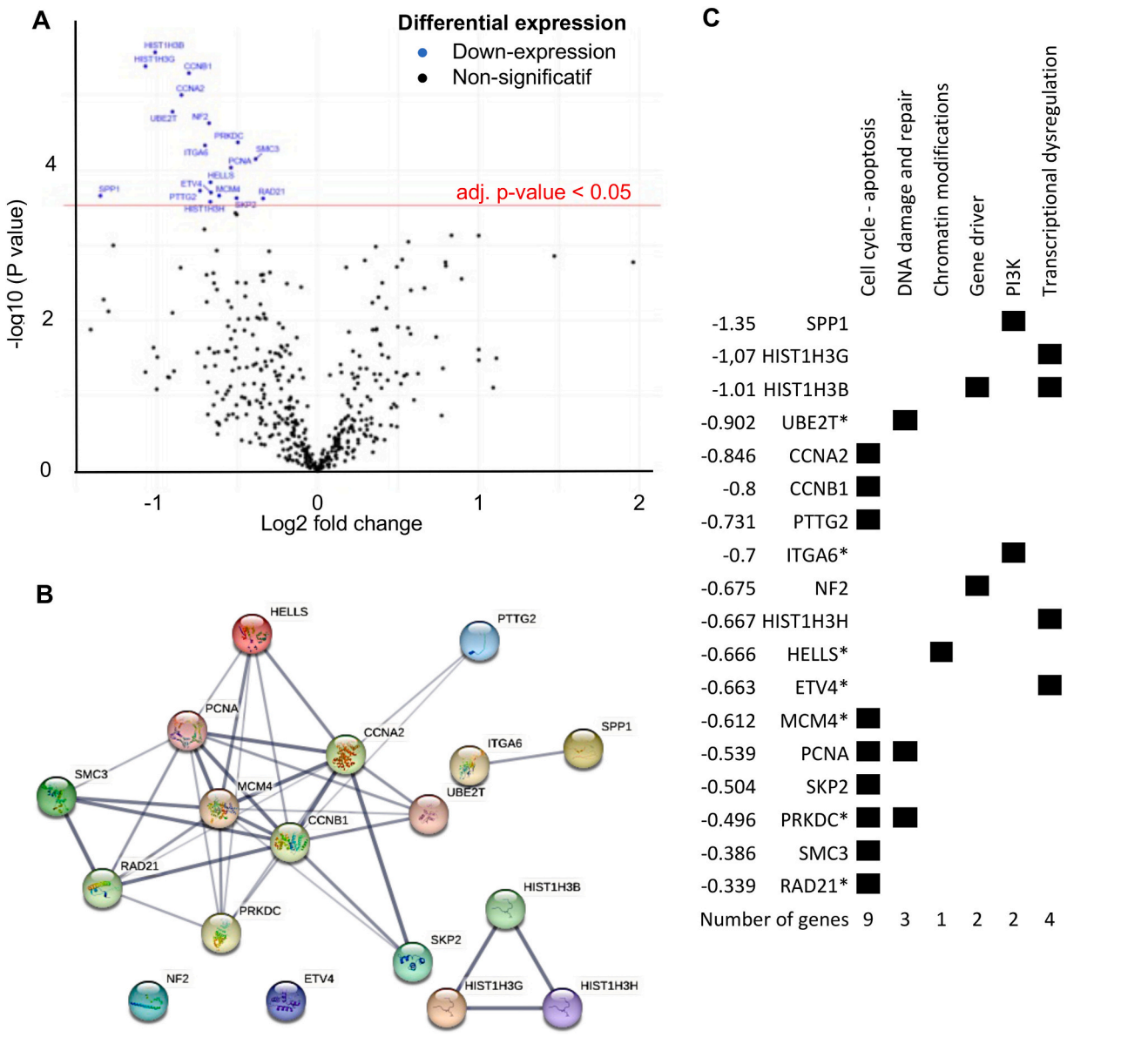

Fig. 4. Detecting a transcriptomic signature of cancer dormancy. DiD-labeled MNNG-HOS cells were cultured in 3D for 35 days before isolating DiD$^+$ and DiD$^-$ cell populations with flow cytometry. (**A**) Transcriptomic signature comparing DiD$^-$ and DiD$^+$ cells obtained by Nanostring™. (**B**) Protein interactions of significantly differentially expressed genes assessed with STRING. (**C**) Signaling pathways associated with differentially expressed genes. Statistical test: *t*-test with Benjamini-Yekutieli *post hoc* test; $p < 0.05$. * correspond to the gene selected for further study.

biological replicates (data not shown). For treatment with the mixture of 5 siRNAs (*HELLS*, *MCM4*, *PRKDC*, *RAD21* and *UBE2T*) called pool, each siRNA was used at a concentration of 2 nM to obtain a final solution concentrated to 10 nM total siRNA. Treatment with siRNAs from the pool condition resulted in extinction coefficients of over 70 % for all target genes apart from *HELLS*. In summary, these results demonstrate the effectiveness of siRNA on gene expression silencing.

Interestingly, treatment with si*ETV4*, si*HELLS*, si*ITGA6*, si*MCM4*, si*PRKDC* and si*UBE2T* was associated with a shift in CI peaks compared with the si*EGFP* control condition (Fig. 5B). Furthermore, cells treated with si*HELLS*, si*ITGA6* and si*UBE2T* showed exponential growth phases identical to the si*EGFP* control condition, but their CI peaks were higher. Cells treated with si*ETV4*, si*MCM4* and si*PRKDC* showed slower exponential growth phases than the si*EGFP* control condition. Furthermore, while conditions treated with si*MCM4* or si*PRKDC* showed CI peaks similar to the si*EGFP* control condition, the treatment with si*ETV4* was associated with a slightly reduced peak. Finally, conditions treated with si*RAD21* and pool had CI curves similar to the untreated condition, with higher, left-shifted CI peaks compared to the si*EGFP* control condition (Fig. 5B).

A comparison of doubling time (Fig. 5C) demonstrated that treatment with si*ETV4* and si*MCM4* significantly increased the time needed to double the CI, while treatment with si*RAD21* significantly decreased it. Furthermore, the CI value at the peak of the curve was significantly higher in the presence of si*RAD21* compared to the si*EGFP*-treated control condition (*$p < 0.05$; Fig. 5D).

Taken together, these results indicate that when the *ETV4* and *MCM4* genes are down-expressed, doubling time increases. Conversely, down-expression of the *RAD21* gene reduces doubling time. In addition, differences in CI height were observed when *RAD21* was down-expressed, as well as a time shift in peak CI for most of the siRNA-treated cells, underlying a potential effect of this specific siRNA on cell morphology or adherence to the substrate.

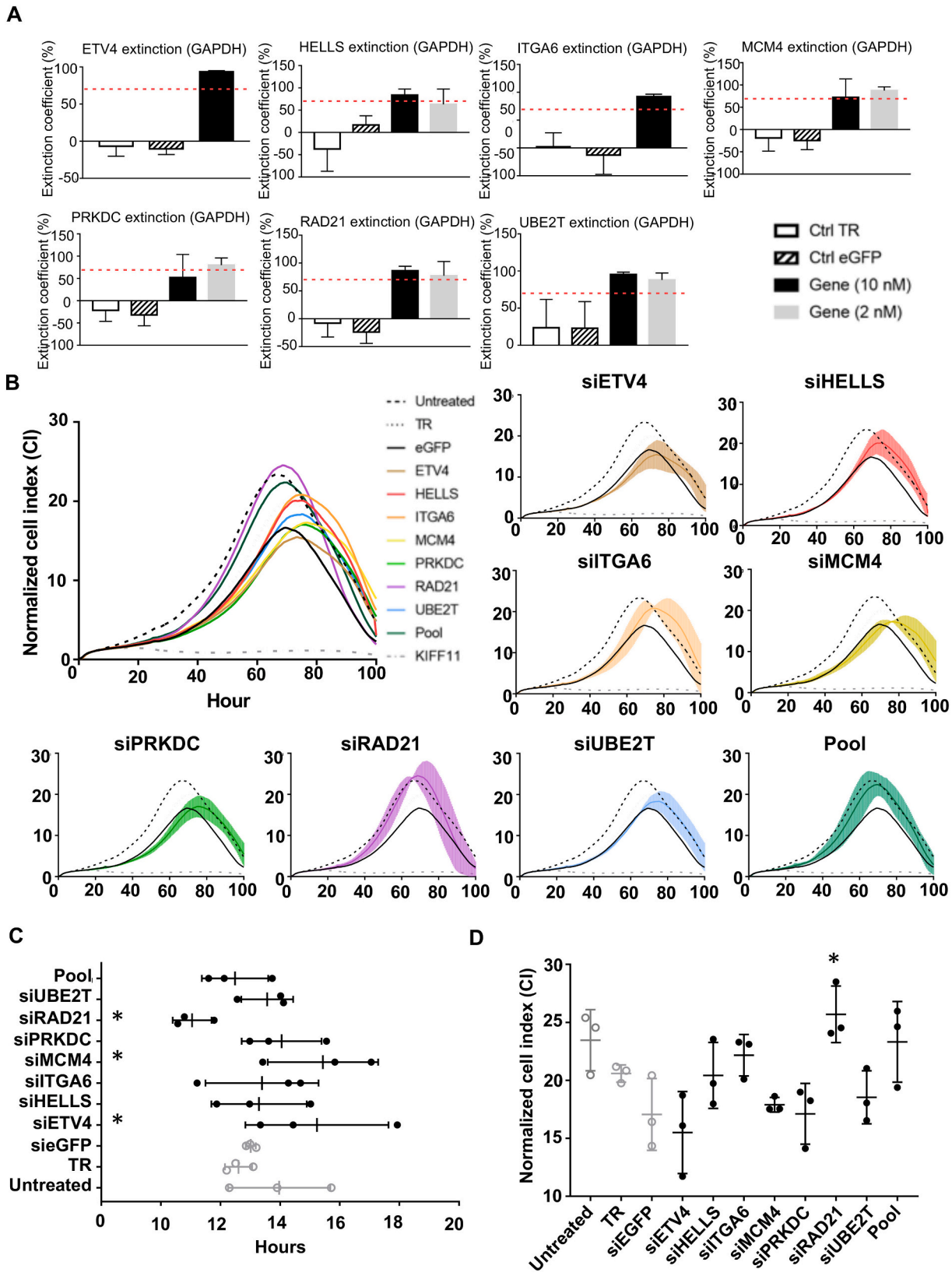

Fig. 5. Evaluating cell proliferation depending on siRNA treatments. MNNG-HOS cells were treated or not with siRNA targeting a transcriptomic signature gene or with a combination of several siRNAs (pool). (**A**) Validating the down-expression of the various genes with RTqPCR. Gene (10 nM) corresponds to siRNA used alone. Gene (2 nM) corresponds to siRNAs used in combination with other siRNAs. (**B**) Normalized Cell Index (CI) measurement of cells cultured in 2D for 100 h by xCELLigence. In the top left, each experimental condition is shown without standard deviations for clarity. Standard deviations are observable for each treatment condition in adjacent graphs. (**C**) Cell doubling time per CI measurement. (**D**) CI value at peak. Statistical test: Mann-Whitney one-sided, comparison with eGFP condition; *$p < 0.05$.

4. Discussion

The present study demonstrates the value of using 3D culture models to investigate the mechanism behind cancer cell dormancy. Long-term culture of osteosarcoma cells labeled with a lipophilic membrane dye that dilutes as cells divide revealed a rapid decrease in fluorescence in 2D cultures, while the dye expression level was maintained in 3D spheroids. This observation indicates that cancer cell proliferation slowed down in 3D cultures. Cancer dormancy is a phenomenon in which cells can enter a state of cell arrest or slowed growth [8]. Dormant cells in cancer also named quiescent cells, cancer stem cells, persister cells or tumor initiating cells remain controversial and should be considered as low cycling cells associated to the resistance of treatment [9]. In view of the results obtained, 3D models appear to be particularly suitable for inducing and studying the mechanisms of cancer cell dormancy.

These disparities in cell proliferation between 2D and 3D cultures can be explained by the spatial organization assumed by the cells in these two culture conditions. Cell lines cultured in 2D proliferate rapidly as long as adherent cells have sufficient space to grow. Under these adherent monolayer culture conditions, cells have equal access to the nutrients and oxygen present in the culture medium. As the culture conditions used (media composition, *etc.*) were favorable for proliferation and cell viability, the cancer cells were subjected to little or no environmental pressure that might otherwise have slowed down their proliferation. Conversely, the 3D organization of spheroids created a centripetal diffusion gradient for nutrients and oxygen, and a centrifugal one for cellular waste [10]. Moreover, depending on the size of the spheroids, a phenotypic stratification of cells could be observed, with a necrotic core, an intermediate layer of cells in cell cycle arrest or slowdown, and a peripheral layer of proliferative cells [11]. For all these reasons, LOT culture of cancer cells encourages cell proliferation to slow down and is therefore relevant for studying mechanisms such as cancer dormancy.

Under LOT culture conditions, spheroids from the different osteosarcoma cell lines showed different morphological profiles. It was thus possible to classify them into three categories: i) large, round spheroids (143B, MNNG-HOS and SJSA-1); ii) intermediate-sized, round spheroids (MG-63) and iii) small, ovoid spheroids (U2OS and SaOS-2). These differences in morphology between cell lines may reflect inter-tumoral variability. Thus, while it is not surprising that the 143B and MNNG-HOS cell lines behaved similarly in 3D given their common origin, the link they share with the SJSA-1 line is less obvious. However, functional characterization of several osteosarcoma cell lines has highlighted the aggressive nature of these three lines. The 143B, MNNG-HOS and SJSA-1 lines showed high tumorigenic, clonogenic, invasive, migratory and proliferative capacities [12,13]. In contrast, the MG-63 cell line shows low or no tumorigenicity, reduced invasiveness and migratory capacity, but high clonogenicity and proliferation. Finally, the U2OS and SaOS-2 lines show similarities in terms of low or non-existent tumorigenicity, intermediate clonogenicity, and invasive and migratory capacities. Their level of proliferation, however, is different: high for the U2OS line, intermediate for the SaOS-2 line [12,13]. Thus, while a correlation between the aggressive nature of the lineage and its ability to form large, round spheres seems to be emerging, it remains difficult to precisely identify a parameter associated with their 3D morphology, especially as the functional characteristics have mostly been described in 2D models. Transposing several of these assays to 3D culture, notably invasion and migration tests, could provide better understanding of the morphological differences observed.

Inducing slowed proliferation and acquiring a cancer dormant phenotype could also be regulated by adding a culture matrix during spheroid generation. Two osteosarcoma cell lines were selected to study the role of both the tumor microenvironment and the extracellular matrix: the MMNG/HOS cell line that forms large spheroids (diameter $>$ 500 μm), and the U2OS cell line that forms smaller spheroids (diameter $<$ 500 μm) when cultured with LOT. In the case of MNNG-HOS cells, adding a culture matrix did not induce morphological variations in the spheroids generated. Conversely, culture of U2OS cells in Geltrex™, a basement membrane matrix extracted from Engelbreth-Holm-Swarm murine tumors, was associated with an increase in the size of the spheroids generated and a decrease in the mean fluorescence intensity of membrane DiD, suggesting an increase in cell proliferation. The value of adding an additive of animal or plant origin to 3D cultures to promote spheroid formation and growth has been demonstrated, in particular for prostate and breast adenocarcinoma cell lines [14–16]. In our study, culture with methylcellulose, a cellulose-derived matrix, did not result in morphological differences compared with LOT culture. Contrary to the conclusions drawn by other authors [16], these results identify the molecular composition of the matrix rather than the viscosity of the additives as the cause of the increased rate of cell proliferation in the case of the U2OS line. Geltrex™ is essentially composed of laminin, collagen IV, entactin and heparan sulfate proteoglycans, which may act as pro-proliferative signals. Moreover, although the product used was selected for its reduced growth factor content, it is likely that some of these molecules are still present in the matrix and play a role in cell proliferation. The extracellular matrix is the sum of these compounds and plays a key role in the progression of osteosarcoma, whether in terms of proliferation, adhesion, invasion or metastasis [17].

More than a month after their seeding in 3D, a cell population still strongly labeled with the lipophilic membrane dye could be detected with flow cytometry, meaning that a number of cells had not proliferated, or had proliferated only slightly, over the entire culture period. Our data are complementary to the works published by Rainusso et al. [18] who used the dye PKH26 to isolate $PKH26^+$ cells after several passages *in vitro* and found that several genes implicated in the cellular acetylation process were downregulated. Interestingly, these authors demonstrated that these cells exhibited some properties of tumor-initiating cells. In our study, after a long-term culture in 3D (35 days without any replating), a comparison of the transcriptomic profile of the DiD^+ population with that of the DiD^- population using the Nanostring™ approach revealed the significant differential expression of 18 genes. Of these genes, 9 are involved in cell cycle pathways. In particular, the under-expression of key players in cell cycle progression such as *CCNA1* and *CCNB2*, as well as several histones involved in DNA compaction, supports the idea that this is a signature of cancer dormancy. In addition to genes with a clear link to cancer dormancy, other genes in this signature also appear to play a more or less direct role in cell proliferation.

Two new regulators of cancer cell dormancy were identified *ETV4* and *MCM4*. *ETV4* is a transcriptional activator, known notably in the context of Ewing sarcomas and prostatic adenocarcinomas to fuse with other genes [19]. In synovial sarcoma, *ETV4* is involved at the cell cycle level, reducing proliferation when under-expressed in tumor cells [20]. Similar results have been described for gastrointestinal or bladder cancers [21,22], where *ETV4* under-expression may be associated with a decrease in cell cycle associated genes and the Wnt/β-catenin signaling pathway, notably by leading to destabilization of β-catenin. β-catenin physiologically translocates into the nucleus and induces transcription of the *CCND1* and *cMYC* genes involved in cell cycle control [22]. Conversely, destabilization of β-catenin by *ETV4* down-expression results in its degradation by the proteasome [23], which explains the reduced proliferation observed *in vivo*. In bladder cancer, *ETV4* plays a role in cell proliferation by binding directly to the promoter region of the *P3H4* gene. Down-expression of *P3H4* leads to a reduction in *CCND1* protein levels *in vitro* and inhibition of tumor growth *in vivo* [21].

ITGA6, a gene encoding an integrin involved in cell adhesion and signaling, also appears to play a role in cell proliferation. A study carried out on osteosarcoma cell lines revealed overexpression of ITGA6 in tumor tissue compared with healthy tissue. *ITGA6* down-expression inhibits osteosarcoma cell proliferation *via* miR-127-3p [24].

RAD21 encodes a subunit of the cohesin complex that ensures the

cohesion of sister chromatids from DNA replication in S-phase to their segregation during mitosis. RAD21 interactome comprises over a hundred molecules, and this protein is involved in numerous other biological pathways such as transcription regulation, apoptosis, and the response to DNA damage [25]. The down-expression of *RAD21* in the MDA-MB-231 breast cancer line induced the appearance of several senescence markers such as β-galactosidase or p21. The acquisition of this senescent phenotype could be the result of the down-expression of c-Myc which would promote activation of the signaling pathway involving RB1, a cell cycle repressor [26].

UBE2T is a protein that not only plays a crucial role in protein degradation processes through the proteasome system but is also involved in the response to DNA damage. Overexpressed in several cancers, such as osteosarcoma, gastric adenocarcinoma, hepatocellular carcinoma and glioblastoma (Heitor [27–30]), *UBE2T* down-expression in osteosarcoma cells inhibits cell proliferation *via* inhibition of the PI3K/AKT signaling pathway [31].

The *HELLS* gene encodes the LSH helicase, involved in DNA strand separation during replication, repair, recombination and transcription. LSH, and by extension HELLS, also plays a role in DNA methylation and chromatin folding. While HELLS has been described as being overexpressed in several sarcomas, including osteosarcoma and soft tissue sarcomas [32,33], as well as in many other cancers [34], its direct role in cell proliferation has yet to be demonstrated in the context of cancer. However, mice genetically modified to have a *HELLS*$^{-/-}$ genotype show an accelerated aging phenotype associated with early and increased replicative senescence [35].

MCM4 is another gene whose direct role in cancer proliferation has not been demonstrated. MCM4 is a protein involved in genome replication. Its expression is increased in several sarcomas [36,37]. In a human fibroblast cell line with proliferation limited to a certain number of cell divisions, MCM4 expression levels drop drastically as senescence approaches [38]. Similar results have been obtained in yeast models [39].

PRKDC is also overexpressed in the context of osteosarcoma [40]. It is the catalytic subunit of the DNA-dependent protein kinase involved in DNA repair by joining non-homologous ends, and phosphorylates the TP53 protein among others. Down-expression of *PRKDC* should therefore be pro-oncogenic, but several studies have highlighted its role in telomere length maintenance. The down-expression of *PKRDC* led to accelerated telomere degradation associated with reduced cell proliferation without increased apoptosis *in vivo* [41]. In addition, PRKDC$^{-/-}$ mice have a shorter lifespan and present age-related pathologies earlier [42]. PRKDC might therefore play a role in replicative senescence.

Overall, and after comparison with data in the literature, we can conclude that the genes differentially expressed in MNNG-HOS DiD^{+} cells are consistent with a dormancy signature.

To verify the role of the *ETV4*, *HELLS, ITGA6, MCM4, PRKDC, RAD21* and *UBE2T* genes in dormancy induction, down-expression of their respective transcripts was induced by RNA interference. Although the transcriptomic signature was obtained from 3D cultures, treatment of spheroids with siRNA raised the problem of diffusion of the molecules within the sphere. In contrast to adherent monolayer cultures, where all cells receive a homogeneous amount of siRNA, 3D culture may induce a diffusion gradient, with cells in the center receiving a much lower concentration of siRNA molecules than those on the periphery. As a result, under-expression is heterogeneous, which could bias the results obtained. Finally, xCELLigence is a simple and direct method for studying cell proliferation, but it is only suitable for adherent monolayer cultures. For all these reasons, the choice was made to validate the effect of down-expression of the various genes of interest in 2D rather than 3D culture.

si*ETV4*, si*MCM4* and si*PRKDC* modulated osteosarcoma CI curves. While *ETV4* had already been described as being involved in regulating cell proliferation [20–22], this is the first time to our knowledge that such a role has been highlighted for *MCM4* and *PRKDC* in the context of cancer and osteosarcoma. Calculating the CI doubling time measured in the exponential phase of growth (between 36 h and 60 h) confirmed the functional contribution of *ETV4* and *MCM4* in controlling cell dormancy *in vitro*.

No difference in the growth phase of the CI curves was observed for cells treated with si*HELLS*, si*ITGA6* or si*UBE2T*. A previous study has already shown that loss of *HELLS* expression had no effect on osteosarcoma cell proliferation [33]. In this context, down-expression of *HELLS* may have cell dormancy as a consequence rather than a cause, which would explain its detection in the transcriptomic signature. In contrast to what has been described in the literature, *ITGA6* and *UBE2T* down-expression does not appear to have an impact on cell proliferation [24,31]. This observation highlights the limitations of the model selected for studying cell proliferation. The transcriptomic signature was obtained from spheroids whose DiD^{+} cells had been in culture for over a month. In the xCELLigence tests, the down-expression of the genes of interest was only studied over a 4-day period. Dormancy induction may be a lengthy process, and the delayed effect of gene under-expression may be lost in our study model.

Finally, the profile of the curves observed in the presence of si*RAD21* and the "pool" condition is the opposite of what was expected initially. These data indicate an acceleration of cell proliferation. A significant decrease in CI doubling time was observed only for cells treated with *RAD21* siRNA. Since the "pool" condition corresponds to an equimolar mixture of si*HELLS*, si*MCM4*, si*PRKDC*, si*RAD21* and si*UBE2T*, each of whose concentrations is 5 times lower than that of cells treated with a single siRNA, it is likely that this leftward shift in the curve is mainly due to the effect of *RAD21* down-expression. Moreover, this shift was associated with a significant increase in CI peak height.

The present work has some limitations. The first limitation of the study is the use of a gene profile from a single osteosarcoma cell line. MNNG-HOS cell line has been chosen as a reference of a large number of publications in the field and for its recognized *in vivo* tumorigeneic properties (growth of primary tumor in bone site with development of lung metastatic foci). We assessed the functionality of the identified genes in 2D culture conditions for three reasons: i) we used transient transfection limiting the duration of the experiments until 72 h and we would like to avoid repeated transfections, ii) the diffusion of siRNA and transfection reagent is reduced in 3D spheroids, and the main risk was to have a siRNA gradient from the periphery to the heart of the spheroids where the DiD^{+} cells were preferentially located, iii) cell proliferation is spontaneously reduced in 3D and we would assess the inhibitory effects of siRNA on cell proliferation explaining why 2D cultures have been preferred. Nevertheless the use of transient transfection reduced the risk to lead to the selection of specific clones compared to stable transduction. Rainusso et al. used the dye PKH26 to select dye positive osteosarcoma cells in 3D cultures. The gene profile identified by these authors does not completely match with the present data. They found that several genes implicated in bone development/inflammation/cell migration were upregulated and genes involved in cellular acetylation process were downregulated. They did not identified the contribution of *ETV4* or *MCM4* which were downregulated in the present work. Complementary works are needed to to assess other osteosarcoma cells lines, cells isolated from patient derived xenografts, and fresh patient samples under the same reported experimental conditions.

In summary, our study demonstrates the relevance of using 3D culture to study mechanisms of tumor progression such as cell dormancy in the context of osteosarcoma. In addition, our results identified *MCM4* and *PRKDC* as new regulators of cell dormancy in osteosarcoma. Cancer dormancy is a complex aspect of cancer biology that plays an important role in tumor progression and treatment resistance [43]. The present study contributes to paving the way for better understanding of cell dormancy in osteosarcoma that may lead to the development of new therapeutic options [44].

Supplementary data to this article can be found online at https://doi.org/10.1016/j.bbamcr.2024.119660.

Abbreviations

LOT Liquid Overlay Technique
2D or 3D cell culture two or three-dimensional cell culture

Ethics approval and consent to participate

NA.

Consent for publication

With the submission of this manuscript we would like to undertake that all authors of this paper have read and approved the final version submitted. We confirm that the contents of this manuscript are not under consideration for publication elsewhere.

Funding

The present works were funded by the French National Angency of Research and Technology (ANRT), Paris (Contract reference: N°2019/1111).

CRediT authorship contribution statement

Camille Jubelin: Writing – review & editing, Writing – original draft, Investigation, Formal analysis. **Javier Muñoz-Garcia:** Writing – review & editing, Validation, Investigation, Formal analysis. **Emilie Ollivier:** Investigation, Formal analysis. **Denis Cochonneau:** Investigation, Formal analysis. **François Vallette:** Writing – review & editing, Visualization, Validation, Formal analysis. **Marie-Françoise Heymann:** Writing – review & editing, Validation, Investigation, Formal analysis. **Lisa Oliver:** Writing – review & editing, Validation, Supervision, Conceptualization. **Dominique Heymann:** Writing – review & editing, Validation, Supervision, Funding acquisition, Conceptualization.

Declaration of competing interest

The authors declare the following financial interests/personal relationships which may be considered as potential competing interests: Atlantic Bone Screen paid the salary of Camille Jubelin. Dominique Heymann is one of the founder and stakeholder of Atlantic Bone Screen.

Data availability

The main data generated and analyzed during this study are included in this published article and its supplementary information files. However, complementary datasets generated during and/or analyzed during the current study are also available from the corresponding author on reasonable request.

Acknowledgements

We thank Prof. Mittnacht for providing the SJSA1 cell line.

References

[1] L. Mirabello, R.J. Troisi, S.A. Savage, International osteosarcoma incidence patterns in children and adolescents, middle ages and elderly persons, Int. J. Cancer 125 (2009) 229–234, https://doi.org/10.1002/ijc.24320.
[2] T.G. Grünewald, M. Alonso, S. Avnet, A. Banito, S. Burdach, F. Cidre-Aranaz, G. Di Pompo, M. Distel, H. Dorado-Garcia, J. Garcia-Castro, L. González-González, A. E. Grigoriadis, M. Kasan, C. Koelsche, M. Krumbholz, F. Lecanda, S. Lemma, D. L. Longo, C. Madrigal-Esquivel, Á. Morales-Molina, J. Musa, S. Ohmura, B. Ory, M. Pereira-Silva, F. Perut, R. Rodriguez, C. Seeling, N. Al Shaaili, S. Shaabani, K. Shiavone, S. Sinha, E.M. Tomazou, M. Trautmann, M. Vela, Y.M. Versleijen-Jonkers, J. Visgauss, M. Zalacain, S.J. Schober, A. Lissat, W.R. English, N. Baldini, D. Heymann, Sarcoma treatment in the era of molecular medicine, EMBO Mol. Med. 12 (11) (2020) e11131, https://doi.org/10.15252/emmm.201911131.
[3] S. Smeland, S.S. Bielack, J. Whelan, M. Bernstein, P. Hogendoorn, M.D. Krailo, R. Gorlick, K.A. Janeway, F.C. Ingleby, J. Anninga, I. Antal, C. Arndt, K.L.B. Brown, T. Butterfass-Bahloul, G. Calaminus, M. Capra, C. Dhooge, M. Eriksson, A. M. Flanagan, G. Friedel, M.C. Gebhardt, H. Gelderblom, R. Goldsby, H.E. Grier, R. Grimer, D.S. Hawkins, S. Hecker-Nolting, K. Sundby Hall, M.S. Isakoff, G. Jovic, T. Kühne, L. Kager, T. von Kalle, E. Kabickova, S. Lang, C.C. Lau, P.J. Leavey, S. L. Lessnick, L. Mascarenhas, R. Mayer-Steinacker, P.A. Meyers, R. Nagarajan, R. L. Randall, P. Reichardt, M. Renard, C. Rechnitzer, C.L. Schwartz, S. Strauss, L. Teot, B. Timmermann, M.R. Sydes, N. Marina, Survival and prognosis with osteosarcoma: outcomes in more than 2000 patients in the EURAMOS-1 (European and American Osteosarcoma Study) cohort, Eur. J. Cancer 109 (2019) 36–50, https://doi.org/10.1016/j.ejca.2018.11.027.
[4] Beird, H.C., Bielack, S.S., Flanagan, A.M., Gill, J., Heymann, D., Janeway, K.A., Livingston, J.A., Roberts, R.D., Strauss, S.J., Gorlick, R., 2022. Osteosarcoma. Nat Rev Dis Primers8(1):77. doi:https://doi.org/10.1038/s41572-022-00409-y.
[5] C. Jubelin, J. Muñoz-Garcia, D. Cochonneau, E. Ollivier, F. Vallette, M. F. Heymann, L. Oliver, D. Heymann, Technical report: liquid overlay technique allows the generation of homogeneous osteosarcoma, glioblastoma, lung and prostate adeno- carcinoma spheroids that can be used for drug cytotoxicity measurements, Front. Bioeng. Biotechnol. 11 (2023) 1260049, https://doi.org/10.3389/fbioe.2023.1260049.
[6] E.C. Jensen, Use of fluorescent probes: their effect on cell biology and limitations, Anat Rec (Hoboken) 295 (2012) 2031–2036, https://doi.org/10.1002/ar.22602.
[7] D. Szklarczyk, R. Kirsch, M. Koutrouli, K. Nastou, F. Mehryary, R. Hachilif, A. L. Gable, T. Fang, N.T. Doncheva, S. Pyysalo, P. Bork, L.J. Jensen, C. von Mering, The STRING database in 2023: protein–protein association networks and functional enrichment analyses for any sequenced genome of interest, Nucleic Acids Res. 51 (2022) D638–D646, https://doi.org/10.1093/nar/gkac1000.
[8] F.M. Vallette, C. Olivier, F. Lézot, L. Oliver, D. Cochonneau, L. Lalier, P.F. Cartron, D. Heymann, Dormant, quiescent, tolerant and persister cells: four synonyms for the same target in cancer, Biochem. Pharmacol. 162 (2019) 169–176, https://doi.org/10.1016/j.bcp. 2018.11.004.
[9] Y. Pu, L. Li, H. Peng, L. Liu, D. Heymann, C. Robert, F. Vallette, S. Shen, Drug-tolerant perister cells in cancer: the cutting edges and future directions, Nat. Rev. Clin. Oncol. 20 (11) (2023) 799–813, https://doi.org/10.1038/s41571-023-00815-5.
[10] C. Jubelin, J. Muñoz-Garcia, L. Griscom, D. Cochonneau, E. Ollivier, M. F. Heymann, F.M. Vallette, L. Oliver, D. Heymann, Three-dimensional in vitro culture models in oncology research, Cell Biosci. 12 (1) (2022) 155, https://doi.org/10.1186/s13578-022-00887-3.
[11] A.P. Browning, J.A. Sharp, R.J. Murphy, G. Gunasingh, B. Lawson, K. Burrage, N. K. Haass, M. Simpson, Quantitative analysis of tumour spheroid structure, eLife 10 (2021) e73020, https://doi.org/10.7554/eLife.73020.
[12] S.U. Lauvrak, E. Munthe, S.H. Kresse, E.W. Stratford, H.M. Namløs, L.A. Meza-Zepeda, O. Myklebost, Functional characterisation of osteosarcoma cell lines and identification of mRNAs and miRNAs associated with aggressive cancer phenotypes, Br. J. Cancer 109 (2013) 2228–2236, https://doi.org/10.1038/bjc.2013.549.
[13] A.B. Mohseny, I. Machado, Y. Cai, K.-L. Schaefer, M. Serra, P.C.W. Hogendoorn, A. Llombart-Bosch, A.-M. Cleton-Jansen, Functional characterization of osteosarcoma cell lines provides representative models to study the human disease, Lab. Investig. 91 (2011) 1195–1205, https://doi.org/10.1038/labinvest.2011.72.
[14] M.A. Badea, M. Balas, A. Hermenean, A. Ciceu, H. Herman, D. Ionita, A. Dinischiotu, Influence of matrigel on single- and multiple-spheroid cultures in breast cancer research, SLAS Discovery 24 (2019) 563–578, https://doi.org/10.1177/2472555219834698.
[15] R. Edmondson, A.F. Adcock, L. Yang, Influence of matrices on 3D-cultured prostate cancer cells' drug response and expression of drug-action associated proteins, PLoS One 11 (2016) e0158116, https://doi.org/10.1371/journal.pone.0158116.
[16] B.M. Leung, S.C. Lesher-Perez, T. Matsuoka, C. Moraes, S. Takayama, Media additives to promote spheroid circularity and compactness in hanging drop platform, Biomater. Sci. 3 (2015) 336–344, https://doi.org/10.1039/c4bm00319e.
[17] J. Cui, D. Dean, F.J. Hornicek, Z. Chen, Z. Duan, The role of extracelluar matrix in osteosarcoma progression and metastasis, J. Exp. Clin. Cancer Res. 39 (2020) 178, https://doi.org/10.1186/s13046-020-01685-w.
[18] N. Rainusso, T.K. Man, C.C. Lau, J. Hicks, J.J. Shen, A. Yu, L.L. Wang, J.M. Rosen, Identification and gene expression profiling of tumor-initiating cells isolated from human osteosarcoma cell lines in an orthotopic mouse model, Cancer Biol. Ther. 12 (4) (2011) 278–287, https://doi.org/10.4161/cbt.12.4.15951.
[19] G.M. Sizemore, J.R. Pitarresi, S. Balakrishnan, M.C. Ostrowski, The ETS family of oncogenic transcription factors in solid tumours, Nat. Rev. Cancer 17 (2017) 337–351, https://doi.org/10.1038/nrc.2017.20.
[20] J. DeSalvo, Y. Ban, L. Li, X. Sun, Z. Jiang, D.A. Kerr, M. Khanlari, M. Boulina, M. R. Capecchi, J.M. Partanen, L. Chen, T. Kondo, D.M. Ornitz, J.C. Trent, J.E. Eid, ETV4 and ETV5 drive synovial sarcoma through cell cycle and DUX4 embryonic pathway control, J. Clin. Invest. 131 (2021) e141908, https://doi.org/10.1172/JCI141908.
[21] L. Hao, K. Pang, H. Pang, J. Zhang, Z. Zhang, H. He, R. Zhou, Z. Shi, C. Han, Knockdown of P3H4 inhibits proliferation and invasion of bladder cancer, Aging (Albany NY) 12 (2020) 2156–2168, https://doi.org/10.18632/aging.102732.
[22] Y. Lecarpentier, O. Schussler, J.-L. Hébert, A. Vallée, Multiple targets of the canonical WNT/β-catenin signaling in cancers, Front. Oncol. 9 (2019).
[23] S. Zeng, A.M. Seifert, J.Q. Zhang, T.S. Kim, T.G. Bowler, M.J. Cavnar, B.D. Medina, G.A. Vitiello, F. Rossi, J.K. Loo, N.J. Param, R.P. DeMatteo, ETV4 collaborates with Wnt/β-catenin signaling to alter cell cycle activity and promote tumor

aggressiveness in gastrointestinal stromal tumor, Oncotarget 8 (2017) 114195–114209, https://doi.org/10.18632/oncotarget.23173.
[24] D. Wang, L. Tang, H. Wu, K. Wang, D. Gu, MiR-127-3p inhibits cell growth and invasiveness by targeting ITGA6 in human osteosarcoma, IUBMB Life 70 (2018) 411–419, https://doi.org/10.1002/iub.1710.
[25] A.K. Panigrahi, N. Zhang, S.K. Otta, D. Pati, A cohesin-RAD21 interactome, Biochem. J. 442 (2012) 661–670, https://doi.org/10.1042/BJ20111745.
[26] S. Zhu, L. Zhao, Y. Li, P. Hou, R. Yao, J. Tan, D. Liu, L. Han, B. Huang, J. Lu, Y. Zhang, Suppression of RAD21 induces senescence of MDA-MB-231 human breast cancer cells through RB1 pathway activation via c-Myc downregulation, J. Cell. Biochem. 117 (2016) 1359–1369, https://doi.org/10.1002/jcb.25426.
[27] Heitor da Silva, J. Maués, H. Ferreira Ribeiro, R. de Maria Maués Sacramento, R. Maia de Sousa, R. Pereira de Tommaso, B. Dourado Kovacs Machado Costa, P. Cardoso Soares, P. Pimentel Assumpção, C. de Fátima Aquino Moreira-Nunes, R. Mário Rodriguez Burbano, Downregulated genes by silencing MYC pathway identified with RNA-SEQ analysis as potential prognostic biomarkers in gastric adenocarcinoma, Aging (Albany NY) 12 (2020) 24651–24670, https://doi.org/10.18632/aging.202260.
[28] P. Huang, Y. Guo, Z. Zhao, W. Ning, H. Wang, C. Gu, M. Zhang, Y. Qu, H. Zhang, Y. Song, UBE2T promotes glioblastoma invasion and migration via stabilizing GRP78 and regulating EMT, Aging (Albany NY) 12 (2020) 10275–10289, https://doi.org/10.18632/aging.103239.
[29] L. Shen, K. Zhao, H. Li, B. Ning, W. Wang, R. Liu, Y. Zhang, A. Zhang, Down-regulation of UBE2T can enhance the radiosensitivity of osteosarcoma in vitro and in vivo, Epigenomics 11 (2019) 1283–1305, https://doi.org/10.2217/epi-2019-0125.
[30] Y. Tao, R. Li, C. Shen, J. Li, Q. Zhang, Z. Ma, F. Wang, Z. Wang, SENP1 is a crucial promotor for hepatocellular carcinoma through deSUMOylation of UBE2T, Aging (Albany NY) 12 (2020) 1563–1576, https://doi.org/10.18632/aging.102700.
[31] Y. Wang, H. Leng, H. Chen, L. Wang, N. Jiang, X. Huo, B. Yu, Knockdown of UBE2T inhibits osteosarcoma cell proliferation, migration, and invasion by suppressing the PI3K/Akt signaling pathway, Oncol. Res. 24 (2016) 361–369, https://doi.org/10.3727/096504016X14685034103310.
[32] W. Huang, Y. Duan, X. Yang, C. Shang, X. Chen, H. Zhang, F. Li, Identification of novel prognostic risk signatures of soft tissue sarcoma based on ferroptosis-related genes, Front. Oncol. 11 (2021) 629868, https://doi.org/10.3389/fonc.2021.629868.
[33] S.C. Wu, C.A. Benavente, Chromatin remodeling protein HELLS is upregulated by inactivation of the RB-E2F pathway and is nonessential for osteosarcoma tumorigenesis, Oncotarget 9 (2018) 32580–32592, https://doi.org/10.18632/oncotarget.25953.
[34] X. Liang, L. Li, Y. Fan, Diagnostic, prognostic, and immunological roles of HELLS in pan-cancer: a bioinformatics analysis, Front. Immunol. 13 (2022) 870726, https://doi.org/10.3389/fimmu.2022.870726.
[35] L.-Q. Sun, D.W. Lee, Q. Zhang, W. Xiao, E.H. Raabe, A. Meeker, D. Miao, D.L. Huso, R.J. Arceci, Growth retardation and premature aging phenotypes in mice with disruption of the SNF2-like gene, PASG, Genes Dev. 18 (2004) 1035–1046, https://doi.org/10.1101/gad.1176104.
[36] Q. Liu, Q. Bao, Y. Xu, Y. Fu, Z. Jin, J. Wang, W. Zhang, Y. Shen, MCM4 is a novel biomarker associated with genomic instability, BRCAness phenotype, and therapeutic potentials in soft-tissue sarcoma, Front. Cell Dev. Biol. 9 (2021) 666376, https://doi.org/10.3389/fcell.2021.666376.
[37] J. Zhou, M. Wang, Z. Zhou, W. Wang, J. Duan, G. Wu, Expression and prognostic value of MCM family genes in osteosarcoma, Front. Mol. Biosci. 8 (2021) 668402, https://doi.org/10.3389/fmolb.2021.668402.
[38] Y. Suzuki, Y. Yamaguchi, H. Hanada, Y. Ishimi, Changes in MCM2-7 proteins at senescence, Genes Genet. Syst. 94 (2019) 123–132, https://doi.org/10.1266/ggs.18-00062.
[39] P.-H. Lee, M.A. Osley, Chromatin structure restricts origin utilization when quiescent cells re-enter the cell cycle, Nucleic Acids Res. 49 (2021) 864–878, https://doi.org/10.1093/nar/gkaa11 48.
[40] T. Mamo, A.C. Mladek, K.L. Shogren, C. Gustafson, S.K. Gupta, S.M. Riester, A. Maran, M. Galindo, A.J. van Wijnen, J.N. Sarkaria, M.J. Yaszemski, Inhibiting DNA-PKCS Radiosensitizes human osteosarcoma cells, Biochem. Biophys. Res. Commun. 486 (2017) 307–313, https://doi.org/10.1016/j.bbrc.2017.03.033.
[41] S. Espejel, S. Franco, A. Sgura, D. Gae, S.M. Bailey, G.E. Taccioli, M.A. Blasco, Functional interaction between DNA-PKcs and telomerase in telomere length maintenance, EMBO J. 21 (2002) 6275–6287, https://doi.org/10.1093/emboj/cdf593.
[42] S. Espejel, M. Martín, P. Klatt, J. Martín-Caballero, J.M. Flores, M.A. Blasco, Shorter telomeres, accelerated ageing and increased lymphoma in DNA-PKcs-deficient mice, EMBO Rep. 5 (2004) 503–509, https://doi.org/10.1038/sj.embor.7400127.
[43] H.K. Brown, M. Tellez-Gabriel, D. Heymann, Cancer stem cells in osteosarcoma, Cancer Lett. 386 (2017) 189–195, https://doi.org/10.1016/j.canlet.2016.11.019.
[44] I. Panez-Toro, J. Muñoz-García, J.W. Vargas-Franco, A. Renodon-Cornière, M. F. Heymann, F. Lézot, D. Heymann, Advances in osteosarcoma, Curr. Osteoporos. Rep, in press (2023), https://doi.org/10.1007/s11914-023-00803-9.